Journal of Non-Crystalline Solids xxx (2012) xxx–xxx

Review

Internal residual stresses in glass-ceramics: A review

Francisco C. Serbena [a,*], Edgar D. Zanotto [b]

[a] Department of Physics, State University of Ponta Grossa (UEPG), CEP 84030-900, Ponta Grossa, PR, Brazil
[b] Vitreous Materials Laboratory (LaMaV), Department of Materials Engineering, Federal University of São Carlos (UFSCar), CEP 13560-970, São Carlos, SP, Brazil

ARTICLE INFO

Article history:
Received 5 December 2011
Received in revised form 18 January 2012
Available online xxxx

Keywords:
Residual stress;
Glass-ceramic;
Glass-matrix composite;
Glass

ABSTRACT

Internal residual stresses arise in glass-ceramics upon cooling down from the crystallization temperature. These stresses are due to the thermal expansion and the elastic mismatch between the crystalline and glassy phases. Therefore, the mechanical properties of glass-ceramics are likely to depend not only on their composition and microstructure but also on the type (tension or compression) and magnitude of these residual stresses. In this work, we critically review the most commonly used theoretical models concerning residual stresses in glass-ceramics and glass-matrix composites, taking into consideration the effects of crystallized volume fraction, crystal shape and thermal expansion anisotropy. We also discuss most of the reported measurements of residual stresses in these dual-phase materials using different techniques, such as X-ray diffraction, nuclear magnetic resonance, Raman and fluorescence spectroscopy, and indentation. The available models and experimental results regarding spontaneous microcracking due to residual stresses are also discussed. Finally, guidelines for future work are suggested.

1. Introduction

Important applications for glass-ceramics have been found in the domestic and high-technology markets [1–3]. Glass-ceramics combine the properties of crystalline ceramics with those of glasses and find applications in the telecommunications and optical industries, such as opto-electronic and microwave devices, surgical implants, dental materials, cooktops, and telescope mirrors [4–6].

Components with complex geometries can be molded in the glass phase at relatively low cost and with relatively simple technology [3]. Then, subsequent heat treatments can partially crystallize the glass object in a controlled manner with a designed microstructure and with very low or no porosity. The crystallized volume fraction can be as low as a few percent or as high as 99.5%. Generally, glass-ceramics have superior optical, chemical, electrical and mechanical properties to those of glasses and similar ceramics that have been produced by sintering.

Glass-ceramics are thus produced by a controlled crystallization that leads to one or more phases embedded within a glassy matrix. Their mechanical, optical and thermal properties depend not only on their composition and microstructure but also on the thermal residual stresses that arise upon cooling due to the thermal and elastic mismatch between the precipitates and the glassy matrix [7]. In addition to these thermal micro stresses, residual macro stresses can arise due to non-homogeneous cooling, leading in some extreme cases to spontaneous cracking [4,6]. Therefore, an understanding of the thermal residual stresses in glass-ceramics and their relationships with the microstructure and overall mechanical properties of the materials is important. The thermal residual stresses may have a significant impact on a material's mechanical performance including its strength [8–11] and stresses in composites [12–14], dental glass-ceramics [15–18] and components of fuel cells [19,20], among other applications.

In this article, we critically review the most popular models for thermal residual stresses in dual-phase materials and their applications in glass-ceramics and glass-matrix composites considering the effects of the thermal and elastic mismatch between the phases, crystallized volume fraction, precipitate shape, thermal expansion anisotropy and microcracking. We then discuss residual stress measurement using X-ray diffraction, nuclear magnetic resonance, Raman and fluorescence spectroscopy and indentation. Finally, we comment on previous experimental studies of microcracking due to residual stresses. The influence of residual stresses on fracture toughness and overall mechanical strength of glass-ceramics [21] will not be considered here.

2. Theoretical models for residual stresses

2.1. The Selsing model

One of the simplest models to estimate internal residual stresses in glass-ceramics is that of Selsing [7]. It assumes that the precipitates (crystals) are spherical and isotropic and that the stress fields around

* Corresponding author at: Universidade Estadual de Ponta Grossa, Departamento de Física, Av. Carlos Cavalcanti, 4748, Ponta Grossa, PR, 84030-900, Brazil. Tel.: +55 42 3220 3044; fax: +55 42 3220 3042.
E-mail address: fserbena@uepg.br (F.C. Serbena).

0022-3093/$ – see front matter © 2012 Elsevier B.V. All rights reserved.
doi:10.1016/j.jnoncrysol.2012.01.040

them do not overlap, which is the case for low crystallized volume fractions (<10%). The stress inside the precipitate, σ_P, is hydrostatic (uniform) and is:

$$\sigma_P = \frac{\Delta\alpha.\Delta T}{K_E} \tag{1}$$

where K_E is $(1+\nu_m)/2E_m + (1-2\nu_p)/E_p$, $\Delta\alpha$ is the thermal expansion mismatch between the precipitate and the matrix, ΔT is the temperature difference between the glass transition temperature (T_g, at which the glass ceases to flow over the laboratory time scale) and room temperature, and E and ν are the elastic constants of the matrix (m) and precipitate (p), respectively. Therefore, the stress inside the precipitate does not depend on the radius, R, of the precipitate.

In the matrix, the radial component, $\sigma_P.R^3/r^3$, has the same sign as σ_P, whereas the two tangential components have the opposite sign and are equal to $-\sigma_P.R^3/2r^3$, as shown in Fig. 1.

2.2. Effect of volume fraction and crystal shape

Generally, glass-ceramics have a crystallized volume fraction higher than 10%; thus, the Selsing model is no longer valid. The effect of the volume fraction on the internal residual stresses has been considered by Mori and Tanaka [23] and Hsueh and Becher [24]. Mori and Tanaka calculated the average stresses in a matrix with inclusions, and Hsueh and Becher, using the Eshelby model for transformation strain on ellipsoidal inclusions embedded in a matrix [25], calculated the residual stresses on inclusions in the form of spheres, fibers and disks, taking their volume fraction into consideration. For spherical precipitates, the stress inside the precipitate is given by:

$$\sigma_p = \frac{\Delta\alpha.\Delta T}{\frac{1}{3K_p} + \frac{1}{4(1-f)G_m} + \frac{f}{3(1-f)K_m}} \tag{2}$$

where G is the shear modulus, K is the bulk modulus and f is the crystallized volume fraction. When $f=0$, this equation becomes the Selsing expression.

The average stress in the matrix ($\bar{\sigma}_m$) is calculated from the equilibrium condition:

$$f.\sigma_p + (1-f).\bar{\sigma}_m = 0. \tag{3}$$

The results of calculations using these equations were compared with simulations carried out by finite element analysis. Higher residual stresses are achieved by large differences in the thermal expansion coefficients and a high elastic modulus. The residual stresses in inclusions decrease with increasing volume fraction in an approximately linear relationship. For the three geometries tested, the highest stresses found are in-plane stresses in disks. The stresses perpendicular to the disk plane are negligible. For fibers, the high-stress component is that along the length of the fiber. Stresses along and perpendicular to their axes remain unchanged for aspect ratios larger than ~5. For spherical inclusions, the magnitude of residual stresses is intermediate between the highest and lowest stress components for disks and fibers.

2.3. Thermal expansion anisotropy

Another factor that influences residual stresses is thermal expansion anisotropy. Crystals with non-cubic symmetry have different thermal expansion coefficients along different crystallographic directions. As a consequence, intergranular stresses arise to accommodate the grain alongside its neighbors, as shown in Fig. 2. This topic has been considered by Evans [26] and Davidge [27] and is described in great detail by Mura [28]. The studies assume a single grain in an infinite isotropic matrix. Inside the grain, different directions have different coefficients of thermal expansion, while the thermal expansion of the matrix is isotropic with average thermal properties equal to those of the grain. This is a reasonable assumption if the grains are randomly oriented. Using the Eshelby model of transformation strains, expressions are obtained for the thermal residual stresses. For example, in a crystal phase with a hexagonal unit cell, the residual stresses are given by the following equations [28–30]:

$$\sigma_a = -\frac{E(7-5\nu)}{45(1+\nu)(1-\nu)}\Delta\alpha.\Delta T \tag{4a}$$

$$\sigma_c = \frac{E(17+5\nu)}{45(1+\nu)(1-\nu)}\Delta\alpha.\Delta T \tag{4b}$$

where σ_a and σ_c are the stresses along the a and c directions and $\Delta\alpha = \alpha_a - \alpha_c$. It is not uncommon to have tensile stresses in one direction inside the grain and compressive stresses in another. These stresses linearly increase with the thermal expansion mismatch due to anisotropy and with increasing elastic modulus.

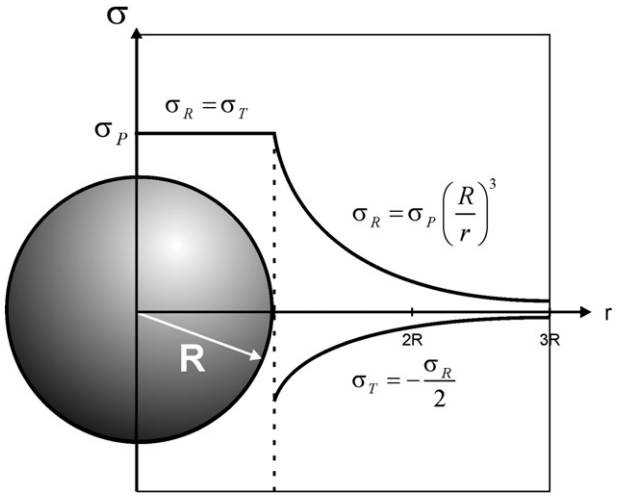

Fig. 1. Stress profiles of a precipitate according to Selsing's model. The stress, σ_P, is constant inside the precipitate. The radial (σ_R) and tangential (σ_T) stress components outside the precipitate decay according to $1/r^3$.
Adapted from Mastelaro and Zanotto [22].

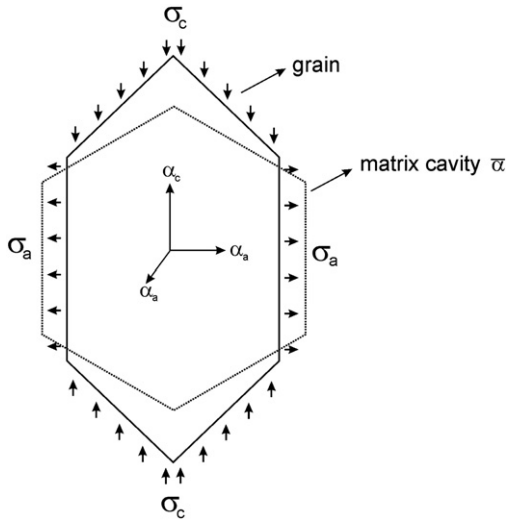

Fig. 2. Unconstrained grain and matrix cavity shapes due to thermal expansion anisotropy. This is a simplified diagram of surface forces acting in the grain for shape conformity.
Adapted from Evans [26].

Please cite this article as: F.C. Serbena, E.D. Zanotto, Internal residual stresses in glass-ceramics: A review, J. Non-Cryst. Solids (2012), doi:10.1016/j.jnoncrysol.2012.01.040

Elastic anisotropy also contributes to the stresses. If the inclusion has elastic constants that vary with crystallographic direction, stresses will arise to accommodate its deformation with the matrix when under load forces. This problem can also be treated using the Eshelby model. Generally, the effect of thermal expansion anisotropy is higher than that of elastic anisotropy [28,29].

2.4. Effect on microcracking

Residual stresses affect the toughness of glass-ceramics. Selsing's model reveals that the residual stresses are tensile in the precipitate when its thermal expansion coefficient is higher than that of the matrix, which is accompanied by tensile radial stresses and compressive tangential stresses in the matrix. A propagating crack will deviate from the precipitates, as shown in Fig. 3(a) [31].

If the residual stresses are compressive on the precipitate, compressive radial stresses and tensile tangential stresses will develop in the matrix. The propagating crack will then be directed toward the precipitates in the matrix and eventually cracking of the precipitates is observed, as shown in Fig. 3(b) [31]. In both cases, residual stresses can change the path of the crack and produce spontaneous microcracking. These observations have important implications on the fracture toughness models for glass-ceramics [32,33].

Residual stresses may thus affect the microcracking of glass-ceramics. Figs. 4 and 5 show the stress distribution inside and outside of a precipitate and the different fracture patterns observed for different combinations of the thermal expansion of a glass and a precipitate. In each case, the tensile stress and the region of lower fracture toughness (matrix or precipitate) control the nucleation and propagation of such microcracks. For the case in which the thermal expansion of the precipitate, α_P, is higher than that of the matrix, α_m, microcracking occurs inside the precipitate if its fracture toughness is lower than that of the matrix, as shown in Fig. 4(b). If the matrix is more brittle, the crack will propagate around the precipitate and inside the matrix due to the tensile radial stress component, as shown in Fig. 4(c). For the case in which α_P is lower than α_m, microcracking occurs in the matrix and links the precipitates due to the tensile tangential matrix stress components, as shown in Fig. 5(a) and (b).

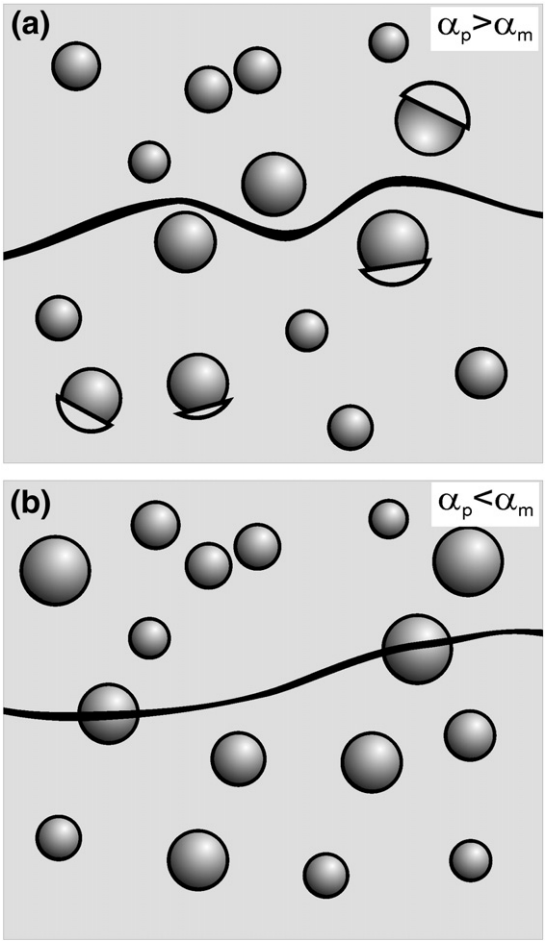

Fig. 3. Schematic crack patterns when (a) the thermal expansion of the precipitate is higher than that of the matrix or (b) the thermal expansion of the precipitate is lower than that of the matrix.
After Davidge and Green [31].

Several models have been proposed for the effect of residual stresses on microfracture. An energy balance exists between the elastic strain energy stored in the precipitate and in the matrix and the energy needed to create new crack surfaces. If the amount of stored mechanical energy is greater than the surface energy, spontaneous cracking occurs; this is related to a critical precipitate radius, R_C.

This critical radius has been calculated for some cases. When the thermal expansion and the fracture toughness of the precipitate are higher than those of the matrix [31], circumferential cracking will occur around the precipitate, as shown in Fig. 4(c). The critical condition is:

$$R_C \geq \frac{4\gamma_S}{K_E.\sigma_P^2}. \tag{5}$$

If the precipitate has a lower K_{IC} value than the matrix, the precipitate will crack as shown in Fig. 4(b), and the critical radius is [30]:

$$R_C \geq \frac{2\gamma_S}{K_E.\sigma_P^2}. \tag{6}$$

For the case in which the thermal expansion of the precipitate is lower than that of the matrix, cracking will occur radially in the matrix, as shown in Fig. 6. The critical radius, as a function of the crystallized volume fraction, was estimated by Todd and Derby [29] based on Green's model [35] and is given by [30]:

$$R_C = \frac{\pi(1-f)^2}{f\left(1-f^{2/3}\right)\left(1+2f^{1/3}\right)^2}\left(\frac{K_{IC}}{\sigma_P^2}\right)^2. \tag{7}$$

If an external stress is applied to a glass-ceramic body, the critical radius for cracking decreases drastically, typically by one order of magnitude, as demonstrated by Green [35].

Another source of microcracking in glass-ceramics (due to residual stresses) is the anisotropic thermal expansion of crystals, which can produce grain-boundary cracking. Defects, such as voids at grain boundaries, act as nucleation sites. Evans [26] estimated the critical grain size (d_g) above which intergranular cracking is observed:

$$d_g = \frac{5.2\,(1+\nu)^2\gamma_{GB}}{E_P(\Delta\alpha.\Delta T)^2} \tag{8}$$

where γ_{GB} is the grain-boundary surface energy and $\Delta\alpha$ is half of the maximum difference in the thermal expansion due to anisotropy. Below the critical grain size, no cracking is observed.

Evidence of grain-boundary microcracking during cooling has been provided by the reduction in the apparent thermal expansion, events of acoustic emission and thermal expansion hysteresis in magnesium and aluminum titanate ceramics [26,36,37].

3. Residual stress measurements in glass-ceramics

Residual stresses in glass-ceramics have been measured using various techniques; among them are X-ray diffraction (XRD), nuclear

Please cite this article as: F.C. Serbena, E.D. Zanotto, Internal residual stresses in glass-ceramics: A review, J. Non-Cryst. Solids (2012), doi:10.1016/j.jnoncrysol.2012.01.040

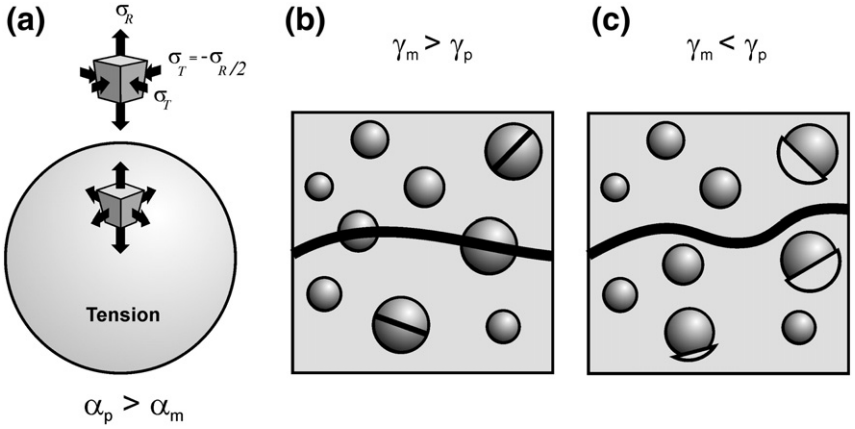

Fig. 4. (a) Thermal residual stress distribution and microcracking for cases in which the thermal expansion of the precipitate is higher than that of the matrix and the matrix surface energy is (b) higher or (c) lower than that of the precipitate. Microcracking of the larger precipitates is represented in (a), and semi-spherical microcracking of the matrix at the precipitate–matrix interface of the larger precipitates is shown in (b).
Adapted from Lange [34].

magnetic resonance (NMR), fluorescence and Raman spectroscopy and indentation.

3.1. Residual stress measurements using XRD

Residual stresses can be measured indirectly using XRD. Reviews on residual stress measurements by XRD can be found in the literature [38–41]. Diffraction is based on Bragg's law, which relates the interplanar distance of a particular *hkl* set of planes with the diffraction angle, θ. Residual strains shift the reflection peaks, which are measured by comparison with those of a stress-free reference sample, usually a finely ground and annealed powder. Sometimes an internal standard, such as alumina or silicon powder, is also used. In this manner, residual strains normal to the *hkl* planes can be measured. Residual stresses can then be calculated from the residual strains using Hooke's law if the elastic constants of the crystal are known.

The full stress tensor can be calculated by measuring the variation of the interplanar distance d_{hkl} of a specific *hkl* plane along at least six independent directions as defined by an azimuthal angle, ϕ, and a tilting angle, ψ. If the principal stress directions are known, only three directions are necessary for the calculation of the full stress tensor.

The other technique involves the use of the Rietveld refinement of high-quality diffractograms of the glass-ceramic in bulk and powder forms. The lattice constants of the crystallized phase are calculated by Rietveld refinement. Several sources of errors, such as sample displacement, roughness, sample transparency, and peak asymmetry, can be considered in the refinement. In addition, all reflections are considered in this method. The unit cell dimensions of the embedded crystals in a monolithic piece of glass-ceramic (the stressed sample) are compared with the unit cell dimensions of the powdered sample (the stress-free sample). In this manner, strains and stresses along any crystallographic direction are obtained.

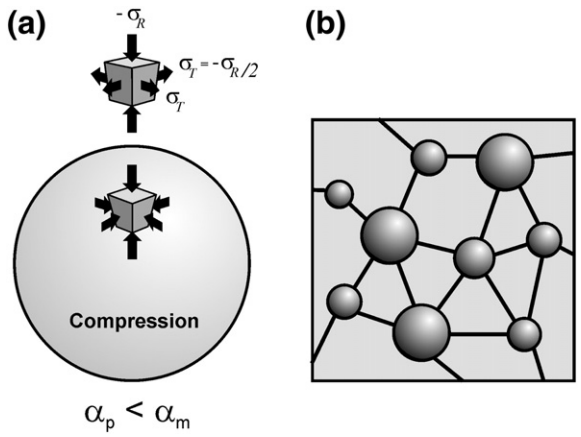

Fig. 5. (a) Thermal residual stress distribution and (b) microcracking in cases in which the thermal expansion of the precipitate is lower than that of the matrix.
Adapted from Lange [34].

Zevin et al. [42] measured the residual stresses in β-eucrypite and β-spodumene solid-solution based glass-ceramics with high crystallized volume fractions. Residual stresses were determined by the peak displacements of several reflections. A powder sample was used as a stress-free reference sample. The measured stresses were anisotropic, and the measured values were much lower than those estimated by Selsing's model. The authors attributed these differences to a pre-existing network of microcracks in the residual glass, but the effect of the high volume fraction of crystal phases was not considered.

Mastelaro and Zanotto [22] measured residual stresses in partially crystallized $1Na_2O{\cdot}2CaO{\cdot}3SiO_2 + 3\%P_2O_5$ glass-ceramics using conventional XRD equipment. Their glass-ceramics had a sufficiently low crystallized volume fraction, in the range of 5–12%, to avoid inter-crystal interaction. Residual strains were measured using the (404) reflection of the low combeite $Na_2Ca_2Si_3O_9$ phase. The experimental residual stress was 150 ± 50 MPa and agreed with the residual stress predicted by Selsing's model of 160 MPa.

Subsequently, the same authors [43] measured residual stresses in a partially crystallized $Li_2O{\cdot}2SiO_2$ glass-ceramic using synchrotron radiation for several crystallographic planes. Their glass-ceramic had a low crystallized volume fraction to avoid percolation of the stress fields. Residual stresses were highly anisotropic and were in agreement with Selsing's model if the thermal expansion anisotropy was considered.

Residual stresses in partially crystallized $Li_2O{\cdot}2SiO_2$ glass-ceramics were also studied by Pinto et al. [44]. High and low energy synchrotron XRD was used to measure residual stresses in the samples with simultaneous internal and surface crystallization. The glass-ceramics investigated had a low crystallized volume fraction. The residual stresses were confirmed to be highly anisotropic in the volume studied, and a good agreement with Selsing's model was obtained if the thermal expansion anisotropy of the $Li_2Si_2O_5$ crystal phase was considered. At the sample surface, the stresses were isotropic and were well predicted by a film model. The average stress was -50 ± 15 MPa in the bulk, and -120 MPa at the surface. The authors suggested that the compressive residual stress at the surface could be used as a strengthening mechanism for improving the mechanical performance of surface-crystallized glass-ceramics [44].

Please cite this article as: F.C. Serbena, E.D. Zanotto, Internal residual stresses in glass-ceramics: A review, J. Non-Cryst. Solids (2012), doi:10.1016/j.jnoncrysol.2012.01.040

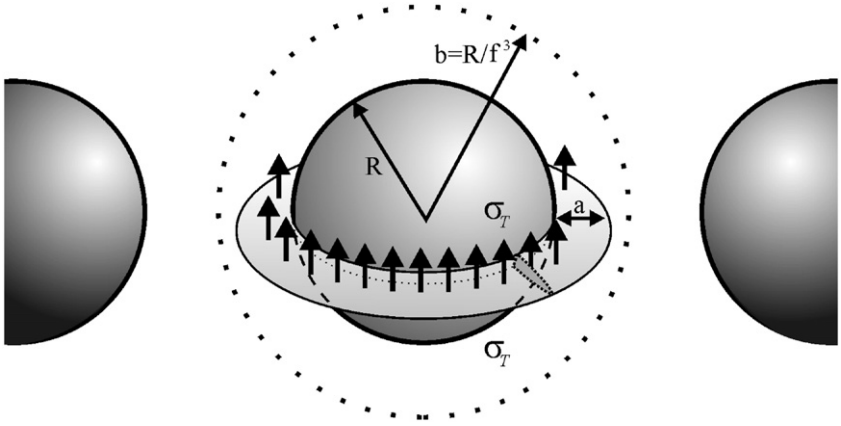

Fig. 6. An annular crack in the matrix growing radially under the tangential residual stress components. Adapted from Todd and Derby [29].

Peitl et al. [45] measured the residual stresses in a partially crystallized $1Na_2O{\cdot}2CaO{\cdot}3SiO_2 + 3\%P_2O_5$ glass-ceramic using XRD. The measured residual stresses confirmed both the previous results of Mastelaro and Zanotto [22] and the validity of Selsing's model for glass-ceramics with low crystallized volume fractions.

Residual stresses in low expansion $Li_2O–Al_2O_3–SiO_2$ (LAS) glass-ceramics produced by sintering and in a commercial LAS glass-ceramic, CERAN®, were measured by Serbena et al. [30] using synchrotron radiation. The crystallized phase is virgilite ($Li_xAl_xSi_{3-x}O_6$). Due to its hexagonal unit cell structure, its thermal expansion is highly anisotropic with contraction along the *c*-direction and almost no thermal expansion along the *a*-direction with increasing temperature. Strains calculated by the Rietveld refinement were in agreement with this thermal expansion anisotropy, showing almost negligible compressive strains along the *a*-directions and fifteen-times higher compressive strains in the *c*-direction. The crystallized volume fractions in the sintered and commercial LAS glass-ceramics were high, approximately 84% and 67%, respectively. The overall residual stresses were low, in the range of −30 MPa to −90 MPa (compression) and could be predicted by taking into account the effect of the volume fraction according to Eqs. (2) and (3). Residual stresses were also measured in a glass with a few isolated crystals nucleated at the surface and in another with a fully covered crystallized surface. The stresses were much higher than in the sintered glass-ceramics but agreed with those calculated by the Selsing and thin film models, respectively.

Residual stresses in a photo-thermo-refractive (PTR) glass-ceramic with a very low volume fraction crystallized (<1%) were measured by Serbena et al. [46] using synchrotron XRD. The crystallized phase was an NaF nanocrystal, and due to its cubic structure, it is isotropic and suitable for investigating Selsing's model with no influence of crystal anisotropy. In addition, the precipitates were nearly spherical and the crystallized volume fraction was very small. The measured thermal residual stresses were quite high, approximately 1 GPa. The experimental results agreed with the calculations of the Selsing model if the significant changes in the glass composition during crystallization – due to Na and F depletion around the crystals – were considered. These changes in composition changed the residual glass thermal expansion coefficient and its T_g value. For glasses heat-treated at higher temperatures, larger dendritic crystals were observed, and the measured residual stresses decreased to 640 MPa. This decrease was attributed to stress relief due to the microcracking of the glass around the precipitates.

In summary, all of the above papers demonstrate that XRD is a successful and accurate technique for measuring the residual stresses in glass-ceramics. The results confirm the validity of Selsing's model [7] for low crystallized volume fraction, and the validity of Hsueh and Becher's model, [47] that considers the effects of the crystallized volume fraction, and the thin film model [30,44]. Conventional XRD is a suitable technique to measure stresses near the sample surface. To measure residual stresses in the sample interior, high energy synchrotron radiation must be used. The use of XRD for stress determination is not suitable for amorphous samples.

3.2. Residual stress measurements using NMR

To the best of our knowledge, the only work published thus far on the measurement of residual stresses by NMR is that of Zwanziger et al. [48], in which the authors have exploited the variations of the NMR resonance frequencies due to variations in the electron distribution for a particular nucleus, the chemical shift. If an applied stress modifies the local bond geometry and bond lengths, the electron distribution is affected and alters the total magnetic field experienced by the nucleus. This, in turn, alters the resonance frequencies in a magnetic field.

The glass-ceramic studied was the PTR glass-ceramic described previously with a low volume fraction of NaF crystals embedded in an oxyfluoride glass matrix. The shifts in the Na and F peaks in the NMR spectra of a partially crystallized glass-ceramic were compared with those of an NaF powder used as a stress-free reference sample. First principle calculations were performed and considered the NaF structure under hydrostatic pressure and the Na and F NMR chemical shifts were calculated as a function of pressure. By comparing the experimental chemical shifts with those predicted by the calculations, stresses in the range of 600–800 MPa were obtained. These values agreed with those predicted by Selsing's model.

Thus, this is a powerful technique that relies on comparing the experimental chemical shifts with those predicted by quantum mechanical calculations. Further experiments with other glass-ceramics must be performed to fully explore the capabilities of this technique.

3.3. Residual stress measurements using Raman and fluorescence spectroscopy

Raman and fluorescence spectroscopy techniques have also been used to measure residual stresses. When a lattice is strained under an applied stress, the energy levels of its electronic and vibrational states are modified, which affects the transition energies and causes slight shifts in frequency as a function of stress [49–52]. Raman spectroscopy is capable of measuring residual stresses and has been used extensively for this purpose in semiconductors [53–55].

Mastelaro and Zanotto [43] attempted to use Raman spectroscopy to measure residual stresses in partially crystallized lithium disilicate glass-ceramics. A calibration curve was constructed by applying pressure to a fully crystallized powder sample using a diamond anvil cell.

Please cite this article as: F.C. Serbena, E.D. Zanotto, Internal residual stresses in glass-ceramics: A review, J. Non-Cryst. Solids (2012), doi:10.1016/j.jnoncrysol.2012.01.040

However, the stress detection limit of their equipment was 150 MPa, which was at the limit of the residual stress variation in their samples (between −120 MPa and +150 MPa).

Raman spectroscopy was also used by Yang and Young [56] to study thermal residual strains in SiC and alumina fibers (with the addition of 20% (wt.%) partially stabilized tetragonal zirconia) embedded in soda-lime silica or Pyrex glass matrices (these materials are not real glass-ceramics but have similar microstructures). Fibers were sandwiched between two plates of glass and hot-pressed at different temperatures in an argon atmosphere. The measured residual strains were proportional to the difference in the thermal expansion of the fiber and the glass matrix, being under either compression or tension depending on whether the thermal expansion of the fiber was smaller or larger than that of the matrix. The residual strains did not depend on the hot-pressing temperature, confirming that the important temperature difference is that between T_g and room temperature. One important observation was made for a Pyrex glass with SiC fiber hot-pressed at 780 °C and subsequently heat-treated at 930 °C for 1 h. The average thermal expansion coefficients of the SiC and Pyrex are nearly the same, $3.1\times10^{-6}\,°C^{-1}$ and $3.2\times10^{-6}\,°C^{-1}$, respectively, suggesting very low residual stresses, but the measured strain in the fiber was 1.8%, the highest measured in the study. Thus, there was some discrepancy between the experimental results and the calculations. However, observations via optical microscopy indicated that the second thermal treatment at 930 °C resulted in the crystallization of the Pyrex glass, matrix microcracking near the fiber-glass interface and a buildup of stress in the fiber. The residual strains along this fiber had a large scatter pattern, indicating that the stresses were not homogeneous along the fiber. It is expected that matrix cracking partially relieves the residual stress. In this case, it seems that glass crystallization near the fiber had induced even higher stresses. However, further studies are necessary to identify the crystallized phase, possible changes in the glass matrix and the fiber and reactions between the fiber and the glass.

In another study, Dassios et al. [57,58] used in situ Raman spectroscopy to study the mechanical behavior of SiC fibers in a LiO_2–MgO–Al_2O_3–SiO_2 glass–ceramic matrix under tensile loading. Strain profiles along individual fibers at different loading stages were measured. Insight into the failure of micro-mechanisms was obtained, and using this technique, the fiber interfacial shear strength was directly measured.

Another technique that has been used is fluorescence spectroscopy. Stress gradients and stresses in very small regions, such as inside grain bridges at a crack surface, were measured using fluorescence spectroscopy [59–61]. One example is the luminescence lines of Cr^{+3} that substitute for Al^{+3} as a dopant in the alumina lattice. Strains in the lattice alter the electronic transitions of the Cr^{+3} ions, and the frequency shift is proportional to the stress. Its piezospectroscopic coefficients have been measured [50].

Young and Yang [62] used fluorescence spectroscopy to measure the residual stresses in single alumina fibers with 20% by weight of tetragonal-stabilized zirconia embedded in a soda-lime glass. The effect of the carbon coating in the fiber was also investigated. The original stress profile, resulting from the thermal expansion mismatch between the fiber and glass matrix, was measured. By applying an external stress, the evolution of the stress along the fiber was observed at different strain levels up to the interface failure and matrix fracture. The applied strain promotes a reduction in the stress level of the fiber. The carbon coating was found to decrease the break-down stress due to the weaker interface when compared with the uncoated fiber.

This technique has also been used by Todd et al. [63] to measure the residual stresses in alumina platelets embedded in a borosilicate glass matrix at different volume fractions up to 30%. The results were compared with the platelet and spherical models of Hsueh and Becher [47] with varying volume fractions. The experimental results were closer to the sphere model than to the platelet model; this observation was attributed to the breaking of the platelets during the milling process.

One advantage of this technique is its capability to sample very small areas (a few micrometers squared) using a confocal microscope. Stress gradients and stresses in very small regions can thus be measured, including inclusions or fibers embedded in a glass matrix (if the glass does not have a Raman or fluorescence peak in the frequency range of interest).

3.4. Residual stress measurements using indentation

Another technique used to determine residual stresses is indentation. This method, first proposed by Zeng and Rowcliffe [64], consists of comparing the length, c_1, of radial cracks produced by an indentation in a stressed region of a specimen with the radial crack length, c_0, made in a stress-free region. The residual stress, σ_m, is given as:

$$\sigma_m = K_{IC}\frac{1-(c_o/c_1)^{3/2}}{\Phi.c_1^{1/2}} \tag{9}$$

where K_{IC} is the stress intensity factor at the indentation crack tip and Φ is a crack geometry factor, which is related to the crack geometry and loading condition and is assumed to be equal to $\pi^{1/2}$. If $c_1 > c_0$, the residual stress, σ_m, is tensile. If $c_1 < c_0$, σ_m is compressive.

Fig. 7 shows a Vickers indentation near a precipitate in a low volume fraction crystallized $17.2Na_2O$–$32.1CaO$–$48.1SiO_2$–$2.5P_2O_5$ (mol%) glass-ceramic [65]. The different crack lengths are related to the tensile radial stresses and the compressive tangential stresses near the precipitate as predicted by the Selsing model.

Nanoindentation has been used by Soares and Lepienski [66] to measure residual stresses around the precipitates in the glass matrix in a low crystallized volume fraction lithium disilicate glass-ceramic. Cracks produced by a Berkovich indenter near the crystals were used, but the calculated residual stresses were lower than those predicted by the Selsing model. It was argued that the method was not appropriate to measure the stresses in a region of approximately 100 μm near the crystal–glass interface because one indentation crack interacted with that of a previous indentation, and smaller cracks (thus smaller indentation loads) were necessary to measure the stresses in that region.

Peitl et al. [45] used the indentation technique to estimate the residual stress distributions in the glass matrix around the precipitates.

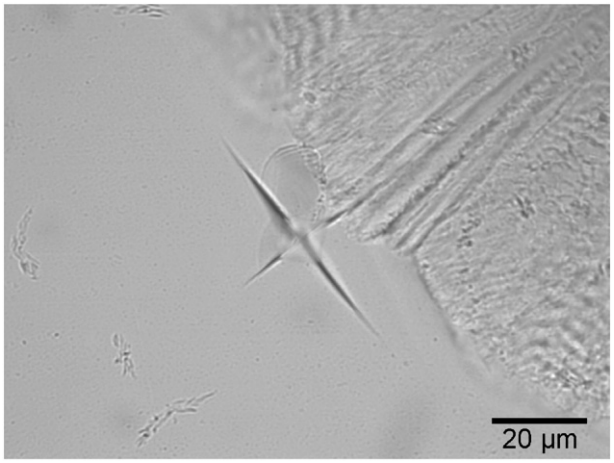

Fig. 7. Optical micrograph of a 0.5 N Vickers indentation around a crystalline precipitate in a $17.2Na_2O$–$32.1CaO$–$48.1SiO_2$–$2.5P_2O_5$ (mol%) glass-ceramic used for the determination of residual stresses.
Reproduced from Peitl et al. [45].

Please cite this article as: F.C. Serbena, E.D. Zanotto, Internal residual stresses in glass-ceramics: A review, J. Non-Cryst. Solids (2012), doi:10.1016/j.jnoncrysol.2012.01.040

A low crystallized volume fraction $17.2Na_2O$–$32.1CaO$–$48.1SiO_2$–$2.5P_2O_5$ (mol%) glass-ceramic was used. Both radial and tangential stress components were measured. The residual stress in the precipitates was also measured using XRD for comparison with the results obtained via the indentation technique. The calculated stresses in the precipitate using Eq. (9), with a value for Φ equal to $\pi^{1/2}$, were approximately 30% of those measured by XRD and predicted by the Selsing model. A careful analysis by sequential polishing revealed that the radial cracks were not semicircular but had a semi-elliptical shape with a length-to-depth ratio of 9.5. This crack geometry required a new crack geometry factor Φ^*. Using fracture mechanics analysis [67], the new crack geometry factor proposed was as follows:

$$\Phi^* = \left(\frac{d_i}{c_i}\right).\left[1.243-0.099\left(\frac{d_i}{c_i}\right)\right]\sqrt{\frac{\pi}{1+1.464\left(\frac{d_i}{c_i}\right)^{1.65}}} \quad (10)$$

where d_i and c_i were the crack depth and radial crack length at the surface, respectively. A reanalysis of the data using the new crack geometry factor restored agreement with the residual stress measured by XRD and predicted by the Selsing model, as shown in Fig. 8(a) and (b).

Therefore, the indentation technique is adequate for measuring residual stresses in glass matrices. It is a fast, inexpensive and non-destructive technique. However, several precautions must be taken for reliable results: the crack shape must be known for the determination of the correct crack geometry factor, indentations must be sufficiently separated so that the stress field of one indentation does not interact with that of another indentation, and the load used must be above a certain threshold to produce cracks because of the finite crack length. This technique has been used in glass-ceramics with large precipitates, but it may not be suitable for glass-ceramics containing very small crystals (<1 μm) or in regions of high stress gradients.

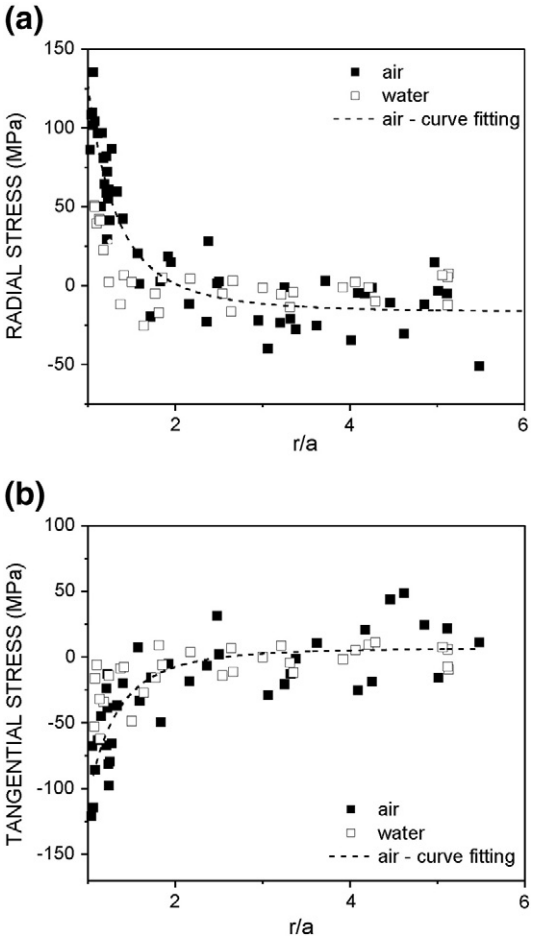

Fig. 8. (a) Radial and (b) tangential stresses as a function of the normalized distance r/a calculated using the indentation technique for indentations in air and water and curve fitted to air data according to Selsing's model.
Reproduced from Peitl et al. [45].

4. Effects of residual stresses on microcracking

The magnitude and sign of the internal residual stresses affect the type of microcracking in glass-ceramics. In Section 2.4 of this paper, we showed that if the precipitate is above a certain critical size, spontaneous microcracking of the precipitate or matrix is observed (depending on the stress sign and the weaker phase).

In their classic work, Davidge and Green [31] studied the strength and microcracking of samples consisting of thorium oxide spheres dispersed in a glass matrix of varying compositions. They observed that if the thermal expansion of the glass was lower than that of the spheres, the cracks contour the spheres and cracks were nucleated around the spheres for precipitates above a certain critical radius. If the thermal expansion of the glass was higher than that of the spheres, radial cracks at the precipitate edges in the matrix were observed, as shown in Fig. 9. Larger precipitates decreased the bending strength, and an externally applied load decreased the sphere's critical radius for microcracking.

Mastelaro and Zanotto [22] also studied the critical radius for spontaneous cracking in a partially crystallized $1Na_2O{\cdot}2CaO{\cdot}3SiO_2 + 3\%P_2O_5$ glass-ceramic. Their glass-ceramic had a low crystallized volume fraction. Different thermal treatments produced particles from 650 μm to 985 μm in diameter. The crystallized phase was a low combeite $Na_2Ca_2Si_3O_9$. Using Eq. (5), a critical size for spontaneous cracking of 88 μm was calculated. However, no spontaneous microcracking was observed in the specimens despite the fact that the experimental precipitate sizes were approximately one order of magnitude larger than the critical size. Though at the time of the experimentation there was no firm explanation for this surprising result, it is now known that there is a significant glass composition gradient around the precipitates in this particular glass-ceramic [69,70]. The crystals are richer in Na and depleted of Ca, and the glass "backyard" surrounding the precipitate is richer in Ca and depleted of Na when compared with the stoichiometric $Na_2Ca_2Si_3O_9$ composition. This fact alters the thermal expansions of the glass and precipitate, increasing the residual stresses in the precipitate [45] and decreasing the critical radius for spontaneous microcracking. However, even this correction is not

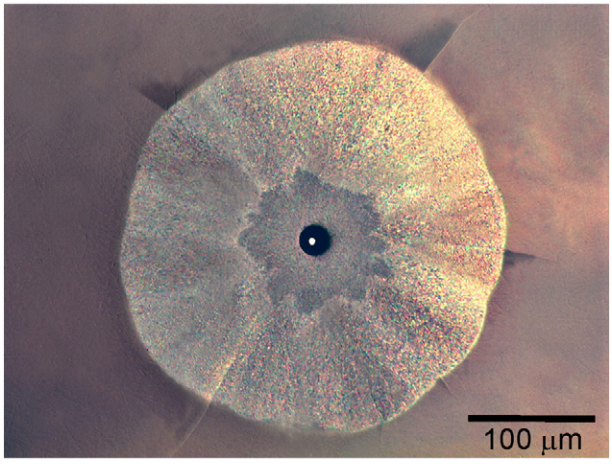

Fig. 9. Optical micrograph of radial cracks generated by a lithium niobate–lithium disilicate double crystal in a glass matrix.
Courtesy of V. O. Soares and M. Crovace [68].

Please cite this article as: F.C. Serbena, E.D. Zanotto, Internal residual stresses in glass-ceramics: A review, J. Non-Cryst. Solids (2012), doi:10.1016/j.jnoncrysol.2012.01.040

enough to quantitatively explain the observed discrepancy. Therefore, no satisfactory explanation exists, and further experimental work must be performed on this glass-ceramic.

The spontaneous radius for microcracking in PTR glass-ceramics has been studied by Serbena et al. [46]. Two different heat treatments produced two types of precipitates: NaF cuboidal nanocrystals (shown in Fig. 10(b)) and larger NaF dendritic micrometer-sized crystals (shown in Fig. 10(d)). The critical diameter for spontaneous microcracking in this glass-ceramic is 2.6 μm, as calculated by Eq. (5), which is about the size of some of the larger dendritic crystals observed by scanning electron microscopy (Fig. 10(d)). Microcracking relieves the residual stresses from ~1 GPa for the cuboidal crystals to 640 MPa for the dendritic crystal (Fig. 10(a) and (c)). Evidence of microcracking was also observed by the presence of two diffraction peaks in the XRD pattern of the glass-ceramics with dendritic crystals. One of the peaks corresponds to a stress of 640 MPa and another to a stress of nearly zero, which is attributed to the microcracked precipitates. The Rietveld refinement analysis reveals that the amount of the "unstressed" NaF precipitates was 25%–30% of the total precipitates.

Spontaneous microcracking has been observed in some glass-ceramics of the Li_2O–Al_2O_3–SiO_2 (LAS) system. The main crystalline phases formed in this system are metastable solid solutions of high-quartz or keatite structure, such as β-spodumene, β-eucryptite and virgilite. All these phases have hexagonal or tetragonal crystal structures and their thermal expansion coefficients are highly anisotropic, with very low or even negative values [71]. These differences cause a crystallographic dependence of the residual stresses, and intergranular stresses in highly crystalline glass-ceramics.

For instance, Sarno and Tomozawa [72] have investigated the mechanical properties of glass-ceramics with $22.2Li_2O$–$18.9Al_2O_3$–$55.9SiO_2$–$3P_2O_5$ (wt.%) with addition of 5 and 15% ZrO_2. By using a two stage heat treatment, 95% crystallinity or higher was achieved. Orthorhombic lithium metasilicate, hexagonal β-eucryptite and tetragonal and monoclinic ZrO_2 were the crystalline phases nucleated. No information was given about the volume fraction of each phase. Different heat treatments produced grain sizes in the range of 0.4–1.4 μm. When the specimens were tested, an increase in fracture toughness with grain size was initially observed. However, for specimens with a grain size larger than ~1 μm, spontaneous cracking was observed. Fracture strength tests also revealed a complete loss of strength for samples with grain size larger than 1 μm. The initial increase in toughness with grain size for the sample without ZrO_2 addition was explained by the formation of microcracks ahead of the crack *during testing*, as proposed by Green [35] and described in Section 2.4. This phenomenon is microcrack toughening, where the microcracks cause dilatation and reduction of the elastic modulus, and both increase fracture toughness [73].

Microcracking was also observed on cooling a sample from the processing temperature for a composition with 15% ZrO_2. The observed microcracking originated from the stresses caused by differences between the thermal expansions of lithium metasilicate and β-eucryptite, and possibly due to their thermal expansion anisotropy. The tetragonal to martensitic transformation of ZrO_2 did not play a role on the mechanical properties of this glass-ceramic.

Sakamoto et al. [74] evaluated the thermal expansion, microstructure and bending strength of β-spodumene glass-ceramics of the LAS system. Two glass-ceramics with slight differences in Li, Ti and Zn oxides were investigated. The crystalline volume fractions were relatively low, around 43%. One of the glass-ceramics had a high value of thermal expansion coefficient that agreed with calculations based on the thermal expansion coefficients of the residual glass and of β-spodumene reported in the literature [71,75]. The other glass-ceramic had a very low thermal expansion, which did not agree with theoretical predictions. Furthermore, it showed mass increase after water immersion, and very low bending strength of 13 ± 2 MPa. SEM observations revealed β-spodumene crystals of 3 to 5 μm in diameter immersed in the residual glass matrix. All these results indicate microstructure microcracking due to the thermal expansion mismatch between the residual glass and the β-spodumene crystals.

Microcracking in virgilite-based low expansion LAS glass-ceramics has been observed by Serbena et al. [30]. A glass-ceramic produced by sintering and a commercial LAS glass-ceramic, CERAN®, were

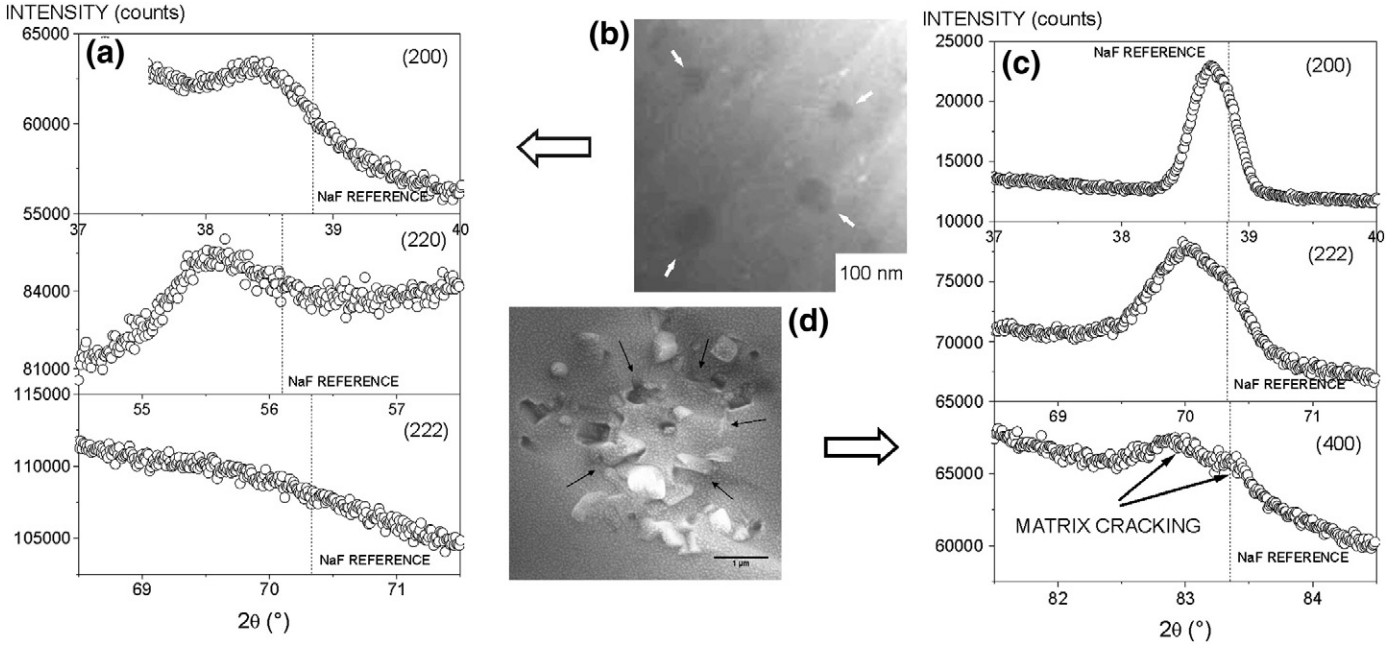

Fig. 10. (a) The XRD pattern of PTR glass, a UV-exposed sample, heat treated for 450 °C—1 h/520 °C—2 h, and the corresponding NaF nano-precipitates (indicated by the arrows); (b) a bright-field TEM image of an exposed PTR glass, heat treated for 483 °C—1 h/515 °C—1 h; (c) the XRD pattern of PTR glass, a UV-exposed sample, heat treated for 450 °C—1 h/650 °C—20 min; and (d) a scanning electron microscopy image of the fractured surface of a PTR sample, unexposed, heat treated at 450 °C—1 h/650 °C—20 min, showing a fractured NaF precipitate and cracks in the surrounding matrix indicated by the arrows.
Reproduced with modifications from Serbena et al. [46].

Please cite this article as: F.C. Serbena, E.D. Zanotto, Internal residual stresses in glass-ceramics: A review, J. Non-Cryst. Solids (2012), doi:10.1016/j.jnoncrysol.2012.01.040

studied. The microstructure of the sintered glass-ceramic consists of large glass particles and smaller rounded virgilite crystals, with diameters of approximately 800 nm, embedded in the residual glass, as shown in Fig. 11(a) and (b). Larger residual glass islands exhibit extensive crack formation and a network of thin cracks. The microstructure of the CERAN® samples consists of very small crystals of virgilite with diameters of 60 nm. No cracks were observed in the CERAN® samples.

Both glass-ceramics exhibit thermal expansion hysteresis. The hysteresis increased after submitting the samples to subsequent thermal shock cycles, as shown in Fig. 12(a) and (b). In each cycle, the sample was heated at 600 °C and quenched to 0 °C for five times. The average thermal expansion of the crystalline phase, as estimated by dilatometry, was different from that measured using high-temperature X-ray diffraction. These facts are all evidence of microstructure microcracking.

The critical size for microcracking of the glass precipitates in the sintered glass-ceramics was estimated using Eq. (6). A critical radius of 11 μm was obtained, which is in good agreement with the size of the observed cracked glass precipitates. Two other possible mechanisms for microcracking of the microstructure were investigated: thermal expansion anisotropy of virgilite and microcracking of the residual glass phase between the virgilite crystals. As the anisotropic thermal expansion of virgilite crystals induced stresses that could produce grain-boundary microcracking, the critical grain size was also estimated for the sintered glass-ceramic. With Eq. (8), a critical grain size of 170 μm was obtained. The critical radius of the virgilite precipitate for spontaneous microcracking was calculated using Eq. (7); a critical radius of 27 μm for the sintered glass-ceramic and 19 μm for CERAN® were calculated. These values were all much higher than the observed virgilite grain size. Therefore, grain-boundary microcracking and microcracking of the residual glass phase are unlikely in these glass-ceramics.

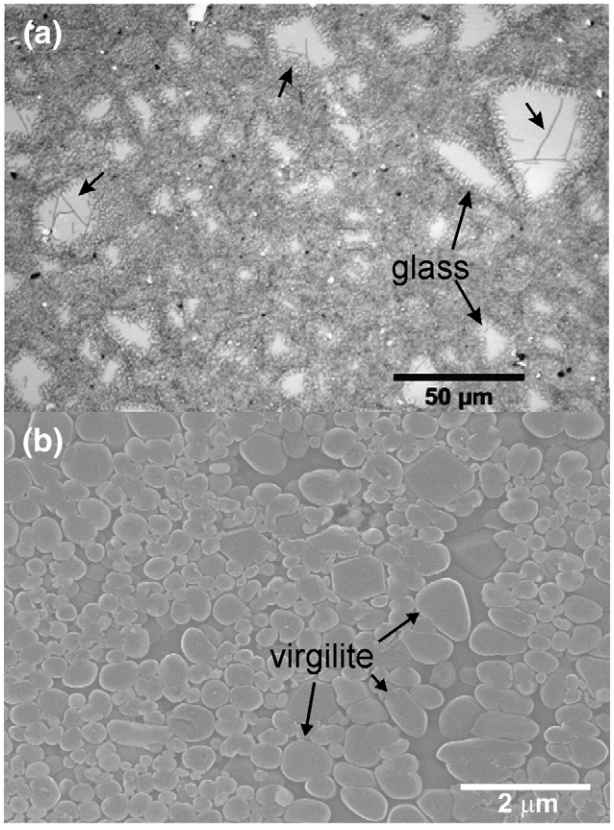

Fig. 11. (a) Microcracking of the larger glass particles as revealed by optical microscopy and (b) the virgilite grains embedded in a glass matrix in the LAS sintered glass-ceramic revealed by SEM. Both samples were etched in a dilute HF solution.
Reproduced from Serbena et al. [30].

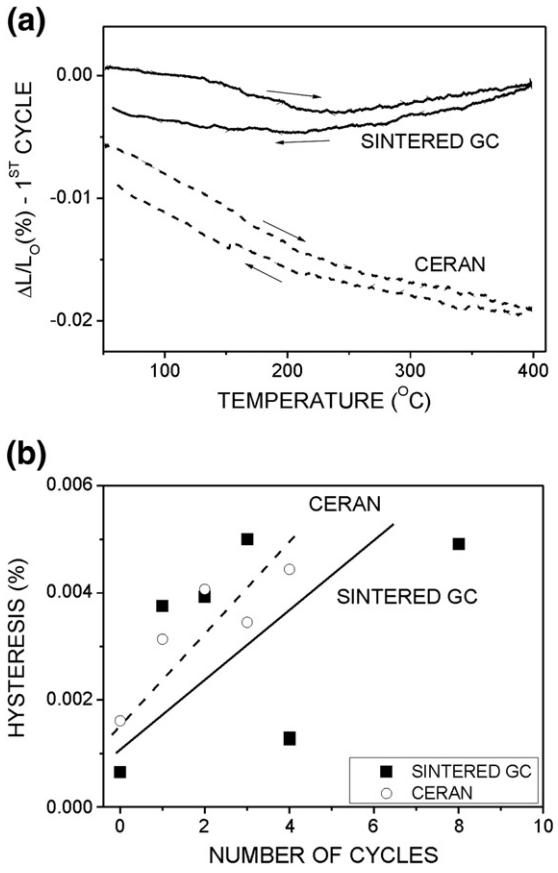

Fig. 12. (a) Thermal expansion hysteresis of the sintered glass-ceramic and CERAN after the first thermal-shock cycle of heating-and-quenching and (b) the accumulated hysteresis as a function of the number of thermal cycles. The lines are added as a guide to the eyes.
Reproduced from Serbena et al. [30].

5. Conclusions

Experiments conducted on some glass-ceramics have shown that Selsing's model can successfully predict the values of internal residual stresses in glass-ceramics containing low crystallized volume fractions. Increasing the crystallized volume fraction reduces the stresses in the crystals, but increases the stresses in the residual glass matrix. The residual stress varies almost linearly with the crystallized volume fraction and depends on the crystal shape. Finally, for non-cubic crystalline phases the thermal expansion anisotropy must be considered, especially for glass-ceramics with high elastic moduli.

Internal residual stresses affecting crack propagation and microcracking is commonly observed in crystals larger than a certain (calculable) critical size. Models based on the strain energy release rate have been largely (but not always) successful in predicting the critical size for microcracking, leaving room for further study.

Several techniques have been used to measure residual stresses in glass-ceramics. XRD and Raman and fluorescence spectroscopy are powerful tools for determining the residual stresses in the crystalline phase, whereas the indentation technique is key for estimating residual stresses in the glass matrix. However, care must be exercised in the determination of the proper conditions under which indentation can be correctly applied. NMR is another powerful technique that requires further exploration.

Valuable lessons can be learned from residual stress determinations and modeling in ceramic composites for use in the design and

Please cite this article as: F.C. Serbena, E.D. Zanotto, Internal residual stresses in glass-ceramics: A review, J. Non-Cryst. Solids (2012), doi:10.1016/j.jnoncrysol.2012.01.040

control of nano- and microstructures in glass-ceramics. New techniques, such as high-energy X-ray microbeam from high-energy synchrotron beam lines and neutron diffraction should be tested for use in the investigation of residual stresses in glass-ceramics.

Despite its great importance, there have been few quantitative studies of residual stresses in glass-ceramics. This is a very interesting and important subject with potential applications including optically transparent, dental and bioactive glass-ceramics. Finally, the effects of internal residual stresses on the overall (macroscopic) mechanical properties of glass-ceramics must still be established.

Acknowledgments

The authors acknowledge CNPq, FAPESP/Brazil-contract nos. 07/08179-9 and 05/53241-9 and the Brazilian Synchrotron Light Laboratory/MCT research proposals XRD1-5824, XRD2-5322, and XRD1-6712 for financial support. We are also indebted to Valmor Mastelaro, Oscar Peitl, Joe Zwanziger, Viviane Soares, Murilo Crovace, Haroldo Pinto, Julien Lumeau and Leon Glebov for most useful discussions on the different measurement techniques that we have tested jointly and used in our previous papers on residual stresses in glass-ceramics.

References

[1] W. Pannhorst, J. Non-Cryst. Solids 219 (1997) 198–204.
[2] G.H. Beall, L.R. Pinckney, J. Am. Ceram. Soc. 82 (1999) 5–16.
[3] E.D. Zanotto, Am. Ceram. Soc. Bull. 89 (2010) 19–27.
[4] P.W. Mc Millan, Glass-Ceramics, 2nd ed. Academic Press, New York, 1979.
[5] J.M.F. Navarro, El Vidrio, 2nd ed. Consejo Superior de Investigaciones Cientificas, Madrid, Spain, 1991.
[6] W. Holand, G.H. Beall, Glass-Ceramic Technology, 1st ed. American Ceramic Society/Wiley, New York, 2002.
[7] J. Selsing, J. Am. Ceram. Soc. 44 (1961) 419-419.
[8] D.G. Grossman, J. Am. Ceram. Soc. 55 (1972) 446–449.
[9] R.F. Cook, B.R. Lawn, T.P. Dabbs, P. Chantikul, J. Am. Ceram. Soc. 64 (1981) C-121–C-122.
[10] R. Chaim, V. Talanker, J. Am. Ceram. Soc. 78 (1995) 166–172.
[11] M. Kotoul, J. Pokluda, P. Sandera, I. Dlouhı, Z. Chlup, A.R. Boccaccini, Acta Mater. 56 (2008) 2908–2918.
[12] A.W. Pryce, P.A. Smith, J. Mater. Sci. 27 (1992) 2695–2704.
[13] K.T. Faber, Annu. Rev. Mater. Sci. 27 (1997) 499–524.
[14] K.-L. Choy, P. Duplock, P.S. Rogers, J. Churchman-Davies, M.T. Pirzada, Mater. Sci. Eng., A 278 (1999) 187–194.
[15] M. Fischer, R. Marx, J. Dent. Res. 80 (2001) 336–339.
[16] B. Taskonak, J.J. Mecholsky Jr., K.J. Anusavice, Biomaterials 26 (2005) 3235–3241.
[17] M.V. Swain, Acta Biomater. 5 (2009) 1668–1677.
[18] I. Denry, J.A. Holloway, Materials 3 (2010) 351–368.
[19] C.-K. Lin, T.-T. Chen, Y.-P. Chyou, L.-K. Chiang, J. Power Sources 164 (2007) 238–251.
[20] J. Malzbender, R.W. Steinbrech, L. Singheiser, Fuel Cells 9 (2009) 785–793.
[21] O. Peitl, E.D. Zanotto, F.C. Serbena, L.L. Hench, Acta Biomater. 8 (2012) 321–332.
[22] V.R. Mastelaro, E.D. Zanotto, J. Non-Cryst. Solids 194 (1996) 297–304.
[23] T. Mori, K. Tanaka, Acta Metall. Mater. 21 (1973) 571–574.
[24] C.H. Hsueh, P.F. Becher, Mater. Sci. Eng., A 212 (1996) 22–28.
[25] J.D. Eshelby, Proc. R. Soc. London, Ser. A 241 (1957) 376–396.
[26] A.G. Evans, Acta Metall. Mater. 26 (1978) 1845–1853.
[27] R. Davidge, Acta Metall. Mater. 29 (1981) 1695–1702.
[28] T. Mura, Micromechanics of Defects in Solids, 2nd ed. Martinus Nijhuff Publisher, Dortrecht, 1987.
[29] R.I. Todd, B. Derby, Acta Mater. 52 (2004) 1621–1629.
[30] F.C. Serbena, V.O. Soares, O. Peitl, H. Pinto, R. Muccillo, E.D. Zanotto, J. Am. Ceram. Soc. 94 (2011) 1206–1214.
[31] R.W. Davidge, T.J. Green, J. Mater. Sci. 3 (1968) 629–634.
[32] K.T. Faber, A.G. Evans, Acta Metall. Mater. 31 (1983) 565–576.
[33] M. Taya, S. Hayashi, A.S. Kobayashi, H.S. Yoon, J. Am. Ceram. Soc. 73 (1990) 1382–1391.
[34] F.F. Lange, Fracture and Fatigue, Academic Press, L.J. Broutman, New York, 1974, p. 1.
[35] D.J. Green, J. Am. Ceram. Soc. 64 (1981) 138–141.
[36] J.A. Kuszyk, R.C. Bradt, J. Am. Ceram. Soc. 56 (1973) 420–423.
[37] Y. Ohya, Z. Nakagawa, K. Hamano, J. Am. Ceram. Soc. 70 (1987) C-184.
[38] I. Noyan, T. Huang, B. York, CRC Cr. Rev. Sol. State 20 (1995) 125–177.
[39] V.M. Hauk, E. Macherauch, Adv. X-Ray Anal. 27 (1983) 81–99.
[40] J. Lu, D. Retraint, J. Strain Anal. Eng. 33 (1998) 127–136.
[41] P.J. Withers, H. Bhadeshia, Mater. Sci. Tech. Ser. 17 (2001) 355–365.
[42] L. Zevin, E. Levi, Z. Bessmertnaya, Inorg. Mater. 13 (1977) 1511–1514.
[43] V.R. Mastelaro, E.D. Zanotto, J. Non-Cryst. Solids 247 (1999) 79–86.
[44] H. Pinto, L. Ito, M. Crovace, E.B. Ferreira, F. Fauth, T. Wroblewski, E.D. Zanotto, A.R. Pyzalla, J. Non-Cryst. Solids 353 (2007) 2307–2317.
[45] O. Peitl, F.C. Serbena, V.R. Mastelaro, E.D. Zanotto, J. Am. Ceram. Soc. 93 (2010) 2359–2368.
[46] F.C. Serbena, G.P. Souza, E.D. Zanotto, J. Lumeau, L. Glebova, L.B. Glebov, J. Am. Ceram. Soc. 94 (2011) 671–674.
[47] C.-H. Hsueh, P.F. Becher, Mater. Sci. Eng., A 212 (1996) 22–28.
[48] J.W. Zwanziger, U. Werner-Zwanziger, E.D. Zanotto, E. Rotari, L.N. Glebova, L.B. Glebov, J.F. Schneider, J. Appl. Phys. 99 (2006) 083511.
[49] Q. Ma, D.R. Clarke, J. Am. Ceram. Soc. 76 (1993) 1433–1440.
[50] J. He, D.R. Clarke, J. Am. Ceram. Soc. 78 (1995) 1347–1353.
[51] L. Schadler, C. Galiotis, Int. Mater. Rev. 40 (1995) 116–134.
[52] I.D. Wolf, Semicond. Sci. Technol. 11 (1996) 139.
[53] Y.B. Gerbig, S.J. Stranick, R.F. Cook, Scr. Mater. 63 (2010) 512–515.
[54] R. Ghisleni, J. Liu, R. Raghavan, P. Brodard, A. Lugstein, K. Wasmer, J. Michler, Philos. Mag. 91 (2011) 1286–1292.
[55] P. Zorabedian, F. Adar, Appl. Phys. Lett. 43 (1983) 177–179.
[56] X. Yang, R. Young, Composites 25 (1994) 488–493.
[57] K.G. Dassios, C. Galiotis, V. Kostopoulos, M. Steen, Acta Mater. 51 (2003) 5359–5373.
[58] K.G. Dassios, C. Galiotis, J. Mater. Res. 21 (2006) 1150–1160.
[59] G. Pezzotti, O. Sbaizero, V. Sergo, N. Muraki, K. Maruyama, T. Nishida, J. Am. Ceram. Soc. 81 (1998) 187–192.
[60] H.Z. Wu, S.G. Roberts, B. Derby, Acta Mater. 56 (2008) 140–149.
[61] S. Guo, R.I. Todd, J. Eur. Ceram. Soc. 30 (2010) 2533–2545.
[62] R. Young, X. Yang, Compos. A 27 (1996) 737–741.
[63] R.I. Todd, A.R. Boccaccini, R. Sinclair, R.B. Yallee, R.J. Young, Acta Mater. 47 (1999) 3233–3240.
[64] K. Zeng, D.J. Rowcliffe, Acta Metall. Mater. 43 (1995) 1935–1943.
[65] O. Peitl, F.C. Serbena, V.R. Mastelaro, E.D. Zanotto, J. Am. Ceram. Soc. 93 (2010) 2359–2368.
[66] J. Soares, C.M. Lepienski, J. Non-Cryst. Solids 348 (2004) 139–143.
[67] M. Murakami, Stress Intensity Factors Handbook, 1st ed. Pergamon, Oxford, 1987.
[68] E.D. Zanotto, Cristais em Vidros: Ciência e Arte, EdUFSCar, Brazil, 2011 (photo in pg. 37 by V.O. Soares and M. Crovace).
[69] V.M. Fokin, O.V. Potapov, E.D. Zanotto, F.M. Spiandorello, V.L. Ugolkov, B.Z. Pevzner, J. Non-Cryst. Solids 331 (2003) 240–253.
[70] V. Fokin, O. Potapov, V. Ugolkov, E.D. Zanotto, F. Spiandorello, Russ. J. Phys. Chem. 77 (2003) 1639–1641.
[71] G. Müller, Low Thermal Expansion Glass Ceramics, Springer-Verlag, H. Bach, Berlin, 1995, pp. 13–25.
[72] R. Sarno, M. Tomozawa, J. Mater. Sci. 30 (1995) 4380–4388.
[73] A.G. Evans, J. Am. Ceram. Soc. 73 (1990) 187–206.
[74] A. Sakamoto, Y. Himei, Y. Hashibe, Adv. Mater. Res. 39 (2008) 381–386.
[75] W. Ostertag, G.R. Fischer, J.P. Williams, J. Am. Ceram. Soc. 51 (1968) 651–654.

Please cite this article as: F.C. Serbena, E.D. Zanotto, Internal residual stresses in glass-ceramics: A review, J. Non-Cryst. Solids (2012), doi:10.1016/j.jnoncrysol.2012.01.040